

1           **Mutations in *MYLPF* cause a novel segmental amyoplasia that manifests as distal**  
2   **arthrogryposis**

3  
4   Jessica X. Chong<sup>1,2,23</sup>, Jared C. Talbot<sup>3,4,22,23\*</sup>, Emily M. Teets<sup>3</sup>, Samantha Previs<sup>5</sup>, Brit L.  
5   Martin<sup>6</sup>, Kathryn M. Shively<sup>1</sup>, Colby T. Marvin<sup>1</sup>, Arthur S. Aylsworth<sup>7</sup>, Reem Saadeh-Haddad<sup>8</sup>,  
6   Ulrich A. Schatz<sup>9</sup>, Francesca Inzana<sup>10</sup>, Tawfeg Ben-Omran<sup>11</sup>, Fatima Almusafri<sup>11</sup>, Mariam Al-  
7   Mulla<sup>11</sup>, Kati J. Buckingham<sup>1</sup>, Tamar Harel<sup>12</sup>, Hagar Mor-Shaked<sup>12</sup>, Periyasamy  
8   Radhakrishnan<sup>13</sup>, Katta M Girisha<sup>13</sup>, Shalini S. Nayak<sup>13</sup>, Anju Shukla<sup>13</sup>, Klaus Dieterich<sup>14,15</sup>,  
9   Julien Faure<sup>15,16</sup>, John Rendu<sup>15,16</sup>, Yline Capri<sup>17</sup>, Xenia Latypova<sup>15,16</sup>, Deborah A. Nickerson<sup>2,18</sup>,  
10   David Warshaw<sup>5</sup>, Paul M. Janssen<sup>6</sup>, University of Washington Center for Mendelian Genomics,  
11   Sharon L. Amacher<sup>3,4,19,20</sup>, Michael J. Bamshad MD<sup>1,2,18,21\*\*</sup>

- 12  
13   1.    Division of Genetic Medicine, Department of Pediatrics, University of Washington, Seattle,  
14        WA 98195, USA.  
15   2.    Brotman-Baty Institute, Seattle, WA, USA.  
16   3.    Department of Molecular Genetics, The Ohio State University, Columbus, OH 43210, USA.  
17   4.    Center for Muscle Health and Neuromuscular Disorders, Columbus OH 43210, USA.  
18   5.    Department of Molecular Physiology and Biophysics, University of Vermont, Burlington,  
19        VT 05405, USA.  
20   6.    Department of Physiology and Cell Biology, The Ohio State University, Columbus OH  
21        43210, USA.  
22   7.    Departments of Pediatrics and Genetics, University of North Carolina, Chapel Hill, NC,  
23        USA.  
24   8.    Division of Genetics, Department of Pediatrics, Medstar Georgetown University Hospital,  
25        Washington DC, USA.  
26   9.    Human Genetics, Medical University, Innsbruck, Austria.

- 27 10. Genetic Counseling Service, Department of Pediatrics, Regional Hospital of Bolzano,  
28 Bolzano, Italy.
- 29 11. Division of Genetic and Genomic Medicine, Sidra Medicine and Hamad Medical  
30 Corporation, Doha, Qatar.
- 31 12. Department of Genetics, Hadassah-Hebrew University Medical Center, Jerusalem, Israel.
- 32 13. Department of Medical Genetics, Kasturba Medical College, Manipal, Manipal Academy of  
33 Higher Education, Manipal, India.
- 34 14. Department of Medical Genetics, CHU Grenoble Alpes, Génétique Médicale, Grenoble,  
35 France.
- 36 15. Université Grenoble Alpes, Inserm, U1216, Grenoble Institut des Neurosciences,  
37 Grenoble, France.
- 38 16. Biochimie Génétique et Moléculaire, CHU Grenoble Alpes, Grenoble, France.
- 39 17. Department of Genetics, APHP-Robert DEBRE University Hospital, UF Génétique clinique,  
40 Paris, France.
- 41 18. Department of Genome Sciences, University of Washington, Seattle, WA 98195, USA.
- 42 19. Dept of Biological Chemistry and Pharmacology, The Ohio State University, Columbus OH  
43 43210 USA.
- 44 20. Center for RNA Biology, The Ohio State University, Columbus OH 43210, USA.
- 45 21. Seattle Children's Hospital, Seattle, WA 98105, USA.
- 46 22. Present address: School of Biology and Ecology, University of Maine, Orono, ME 04469,  
47 USA.
- 48 23. These authors contributed equally to this work

49

50

51 **Corresponding authors:**

52 **\*\*Mike Bamshad, MD**

53 Department of Pediatrics  
54 University of Washington School of Medicine  
55 Box 357371  
56 1959 NE Pacific Street, HSB I607  
57 Seattle, WA 98195  
58 Phone: (206) 221-4131  
59 FAX: (206) 221-3795  
60 [mbamshad@uw.edu](mailto:mbamshad@uw.edu)

61  
62 \*Jared C. Talbot, PhD  
63 School of Biology and Ecology  
64 University of Maine  
65 5735 Hitchner hall  
66 Orono, ME 04469  
67 Phone: (207) 581-2835  
68 [jared.talbot@maine.edu](mailto:jared.talbot@maine.edu)

69  
70  
71

72 **Abstract**

73 We identified ten persons in six consanguineous families with Distal Arthrogyryposis (DA) who  
74 had congenital contractures, scoliosis, and short stature. Exome sequencing revealed that each  
75 affected person was homozygous for one of two different rare variants (c.470G>T,  
76 p.(Cys157Phe) or c.469T>C, p.(Cys157Arg)) affecting the same residue of *myosin light chain*,  
77 *phosphorylatable, fast skeletal muscle (MYLPF)*. In a seventh family, a c.487G>A,  
78 p.(Gly163Ser) variant in *MYLPF* arose *de novo* in a father, who transmitted it to his son. In an  
79 eighth family comprised of seven individuals with dominantly-inherited DA, a c.98C>T,  
80 p.(Ala33Val) variant segregated in all four persons tested. Variants in *MYLPF* underlie both  
81 dominant and recessively inherited DA. Mylpf protein models suggest that the residues  
82 associated with dominant DA interact with myosin whereas the residues altered in families with  
83 recessive DA only indirectly impair this interaction. Pathological and histological exam of a foot  
84 amputated from an affected child revealed complete absence of skeletal muscle (i.e., segmental  
85 amyoplasia). To investigate the mechanism for this finding, we generated an animal model for  
86 partial MYLPF impairment by knocking out zebrafish *mylpfa*. The *mylpfa* mutant had reduced  
87 trunk contractile force and complete pectoral fin paralysis, demonstrating that *mylpf* impairment  
88 most severely affects limb movement. *mylpfa* mutant muscle weakness was most pronounced  
89 in an appendicular muscle and was explained by reduced myosin activity and fiber  
90 degeneration. Collectively, our findings demonstrate that partial loss of MYLPF function can  
91 lead to congenital contractures, likely as a result of degeneration of skeletal muscle in the distal  
92 limb.

93

94

95 **KEYWORDS**

96 exome sequencing, Mendelian disease, congenital contractures, distal arthrogyryposis,  
97 amyoplasia, development, skeletal muscle, zebrafish

## 98 Introduction

99 The distal arthrogyroses (DA) are a group of Mendelian conditions with overlapping  
100 phenotypic characteristics, shared genetic etiologies, and similar pathogenesis.<sup>1</sup> Clinically, the  
101 DAs are characterized by non-progressive congenital contractures of the limbs, most commonly  
102 affecting the hands, wrists, feet, and ankles. Congenital contractures of the face, ocular  
103 muscles, neck webbing, pterygia, short stature, and scoliosis are less frequent, variable findings  
104 that facilitate delineation among the most common DA conditions: DA1<sup>2</sup> (MIM 108120), DA2A<sup>3</sup>  
105 (Freeman-Sheldon syndrome [MIM 193700]) and DA2B<sup>4</sup> (Sheldon-Hall syndrome [601680]).  
106 Variants in any one of sixteen different genes can underlie DA but the overwhelming majority of  
107 known pathogenic variants occur in just five genes (*TPM2* (MIM 190990), *TNNI2* (MIM 191043),  
108 *TNNT3* (MIM 600692), *MYH3* (MIM 160720), *MYH8* (MIM 160741)).<sup>5,6</sup> Yet, collectively  
109 pathogenic variants are identified in only ~60% of families diagnosed with a DA, so the precise  
110 genetic etiology remains unknown in nearly half of DA families.

111 Most of the genes that underlie DA encode sarcomeric components of skeletal muscle  
112 fibers. Thus, genes encoding sarcomeric proteins have long been considered priority candidates  
113 for DA. Sarcomeres are the fundamental contractile structure of muscle, wherein myosin-rich  
114 thick filaments interact with actin-based thin filaments to generate contractile force. Each  
115 skeletal muscle myosin heavy chain protein (MyHC) has two distinct light chain proteins bound  
116 to the myosin lever arm: an essential light chain that is nearest to the myosin head, and a  
117 regulatory light chain protein that can be phosphorylated and is located closer to the myosin tail  
118 region.<sup>7</sup> Light chain proteins are needed to stabilize the myosin lever arm so that myosin can  
119 generate maximum force and velocity as revealed by in vitro studies of isolated myosin extracts  
120 deficient in light chain proteins.<sup>8,9</sup>

121 To discover novel genes underlying DA, we performed exome sequencing (ES) on 172  
122 families in which pathological variants in genes known to underlie DA1, DA2A, and DA2B had

123 not been identified via Sanger sequencing. We identified putative pathogenic variants in 80  
124 (47%) of these families including 44 families with mutations in 20 genes not known to underlie  
125 DA. Affected individuals from two families, including an affected child (Family B) who had  
126 complete absence of skeletal muscle (i.e., segmental amyoplasia) in a foot (Figure 1), were  
127 each homozygous for the same variant (c.470G>T) in the gene, *MYLPF*, which encodes the  
128 fast-type skeletal muscle regulatory light chain. Data sharing via MatchMaker Exchange (MME)  
129 and directly with commercial diagnostic labs identified six additional families with similar  
130 phenotypic features and rare variants in *MYLPF*, including two families in which the condition  
131 was transmitted from parent to offspring (Table 1, Families G and H). The mouse *Mylpf*  
132 knockout mutant is born without skeletal muscle and dies soon after birth because of respiratory  
133 failure,<sup>10</sup> suggesting that human pathogenic *MYLPF* variants are likely to be hypomorphic  
134 alleles. To test this hypothesis, we knocked out the more prominent of the two zebrafish *mylpf*  
135 genes, *mylpfa*, and characterized development and function of *mylpfa* mutant skeletal muscle.

136 Zebrafish are a well-established model for investigating muscle structure, development,  
137 and disease mechanisms.<sup>11–14</sup> Zebrafish rapidly generate functional myofibers that produce both  
138 spontaneous and evoked contractions at one day post-fertilization (dpf). By this stage, muscle  
139 fiber type is also readily apparent, with fast-twitch muscles identified by expression of *mylpfa*  
140 and other markers.<sup>15–18</sup> Between 1 and 3 dpf, muscle precursors migrate away from their origin  
141 to produce new *mylpfa*-positive muscles, including fin muscles and the posterior hypaxial  
142 muscle.<sup>19–23</sup> Herein, we show that partial loss of *Mylpf* function in zebrafish can recapitulate  
143 DA1, demonstrate that variants in *MYLPF* underlie DA1, and use a zebrafish model to provide  
144 explanations for the limb muscle loss observed in DA1 due to pathogenic variants in *MYLPF*.

145

## 146 **Materials and Methods**

### 147 *Discovery Cohort*

148 From our cohort of 463 families (1,582 individuals) with multiple congenital contractures, we  
149 selected 172 families in which pathological variants had not been identified. All studies were  
150 approved by the institutional review boards of the University of Washington and Seattle  
151 Children's Hospital and informed consent was obtained from each participant or their parents.

152

### 153 *Exome Sequencing and Variant Analysis*

154 ES was performed by the University of Washington Center for Mendelian Genomics as  
155 described previously.<sup>24</sup> In brief, data were annotated with the Variant Effect Predictor v89<sup>25</sup> and  
156 analyzed using GEMINI 0.20.2.<sup>26</sup> Variants unlikely to impact protein-coding sequence (for which  
157 GEMINI impact\_severity = LOW), variants flagged by the Genome Analysis Toolkit (GATK) as  
158 low quality, and variants with an alternative allele frequency > 0.005 in any super-population in  
159 EVS/ESP6500, 1000 Genomes (phase 3 release), or the gnomAD Browser (v.2.0.1) were  
160 excluded. Variants that were frequent (alternative allele frequency >0.5) in an internal database  
161 of >7,500 individuals (Geno2MP v1.7 release) were excluded. Candidate genes were identified  
162 by filtering under these parameters for variants matching the predicted pattern of inheritance  
163 (i.e. autosomal *de novo*, homozygous recessive, compound heterozygous, X-linked *de novo*, X-  
164 linked recessive, and X-linked dominant models).

165

### 166 *Fish maintenance and husbandry, transgenes, and mutant construction*

167 All animal protocols used in this study are approved by the Institutional Animal Care and Use  
168 Committees at The Ohio State University, the University of Vermont, and the University of  
169 Maine. Standard practices were used for zebrafish husbandry and maintenance.<sup>27</sup> Transgenic  
170 and mutant zebrafish strains were maintained on the AB wild-type background. Transgenic lines  
171 used in this study are *Tg(mylpfa:lyn-Cyan)fb122*,<sup>28</sup> *Tg(myog:Hsa.HIST1H2BJ-mRFP)fb121*  
172 (abbreviated *myog:H2B-mRFP*),<sup>29</sup> and *Tg(smyhc1:EGFP)i104*,<sup>30</sup> which are combined in a

173 '3MuscleGlow' triple-transgenic line.<sup>31</sup> The two *mylpfa* mutant lines described in this study were  
174 generated using established CRISPR/Cas9 protocols.<sup>32</sup> One-cell embryos were injected with  
175 Cas9 mRNA and guide RNA targeting Exon 2 (5'-TTGAGGCCAACACGTCCCTA-3') or Exon 3  
176 (5'-GGTGAAGTTGATTGGGCCGC-3'), raised to adulthood, and outcrossed. F1 progeny were  
177 screened using HRMA to identify founders carrying CRISPR-induced *mylpfa*<sup>oz43</sup> and *mylpfa*<sup>oz30</sup>  
178 lesions. All lesions were sequence confirmed in homozygotes. Mutations were outcrossed at  
179 least two generations after CRISPR injection before phenotypic analyses.

180

#### 181 *Zebrafish Immunohistochemistry and RNA in situ hybridization*

182 Embryos and larvae carrying the *Tg(smyhc1:EGFP)i104* transgene were fixed and  
183 immunolabeled with Rbfox1l (1:500)<sup>33</sup> and F310 (1:100, Developmental Studies Hybridoma  
184 Bank) antibodies. RNA in situ hybridization was performed as described<sup>34</sup> using *mylpfa*<sup>18</sup> and  
185 *mylpfb* riboprobes. For the latter, a 408 bp *mylpfb* fragment was amplified from zebrafish cDNA  
186 using forward 5'-AGTGGCCCCATCAACTTTACTG-3' and reverse 5'-  
187 AGCCCAAATGCCAACAAACC-3' primers and cloned into a PCR4-TOPO vector for  
188 subsequent probe synthesis.

189

#### 190 *Live imaging of muscle structure*

191 The following transgenes were used for live imaging: *Tg(mylpfa:lyn-Cyan)fb122*<sup>28</sup> to visualize  
192 fast muscle membranes, *Tg(myog:H2B-mRFP)*<sup>29</sup> to visualize myonuclei, and  
193 *Tg(smyhc1:EGFP)i104*<sup>30</sup> to visualize slow muscle fibers. Time-lapse imaging was performed as  
194 described.<sup>23</sup> For 3.25 dpf (78 hpf) and 4.25 dpf (102 hpf) comparisons, fish were dismantled  
195 and raised at 28.5°C between imaging sessions.

196

#### 197 *Muscle Contractile Force Measurement*



198 Contractile analysis of 3 dpf larvae was performed as described previously.<sup>35</sup> Live 3 dpf larvae  
199 were anesthetized in 0.02% weight/volume tricaine buffered with Tris-HCl in Krebs-Henseleit  
200 solution and mounted on a custom-built set up between a force transducer and a hook. Larvae  
201 were stimulated at increasing frequencies and contractile strength measured. The maximal  
202 contractile force reached during each contraction was recorded, analyzed, and reported per  
203 larva. Fused tetanic contractions occur at 180 Hz. Measurements were compared at each  
204 contraction frequency using ANOVA followed by Tukey-Kramer post-hoc comparisons.

205

### 206 *Behavioral analysis*

207 To quantify fin movement, we recorded fish for one full minute, recorded the number of beats on  
208 each side of the fish, and then averaged fin movements per side. Escape response was evoked  
209 by gentle probing.<sup>36</sup> Freely moving fish were imaged using a Leica DMC5400 camera mounted  
210 on a Leica MZ10F microscope; images were collected in LAS X software and processed in FIJI.

211

### 212 *Assessing Isolated Myosin Molecular Function*

213 Zebrafish carrying *mylpfa*<sup>oz30</sup> and *mylpfa*<sup>oz43</sup> mutations were intercrossed, raised to 2 dpf, and  
214 sorted for wild-type or mutant swimming behavior. Proper sorting of mutant versus wild-type  
215 sibling embryo genotypes was confirmed on over 100 fish per group. At 4 dpf, fish were  
216 prepared, myosin extracted, and the *in vitro* motility assay was performed as described in the  
217 Supplementary Methods. Fish were dechorionated, de-yolked, permeabilized, and cut open  
218 through the abdomen to expose the de-membranated muscle fibers to subsequent solutions.  
219 Two fish larvae were inserted, tail first, into a flow cell constructed from a microscope slide and  
220 coverslip, as described previously.<sup>37</sup> Myosin Extraction Buffer was infused and incubated for  
221 one hour, followed by 0.5mg/ml BSA in Actin Buffer and incubated for 2 minutes at 30°C. All  
222 solution changes after this point were identical to that previously reported.<sup>38</sup> In brief, unlabeled

223 actin was infused to effectively eliminate non-functional myosin heads, and then followed by  
224 rhodamine-phalloidin labeled actin in Motility Buffer containing ATP. Imaging and actin filament  
225 tracking and velocity analysis were conducted as previously described.<sup>39</sup> Each flow cell  
226 contained myosin from two fish, and at least four fields of view were imaged with at least 20  
227 fluorescent actin filaments tracked per field. Velocity of these tracks was averaged across all  
228 fields of view for a single statistical N. Experiments for a given group were repeated on 4 flow  
229 cells minimum with at least two fully independent replicates on separate imaging days. For  
230 illustrative purposes in Figure 3L and Movie S3, actin filaments were tracked using the MTrackJ  
231 function in FIJI. Actin filament particles that stayed in the viewing frame throughout 100 frames  
232 of imaging were randomly selected and tracked for both wild-type sibling and *mylpfa*<sup>oz30</sup> mutant  
233 genotypes.

234

### 235 *Protein analysis*

236 Protein models were downloaded from PDB and visualized using Geneious software. Structures  
237 shown have the following PDB accession numbers: scallop IKK7;<sup>40</sup> Squid 3I5H;<sup>41</sup> Chicken  
238 2W4G;<sup>42</sup> Rabbit, 5H53.<sup>43</sup> Protein alignments were produced by a MUSCLE algorithm in  
239 Geneious software. Protein sequences with the following accession numbers were downloaded  
240 from NCBI, Ensembl, or Uniprot: human MYLPP (NP\_037424.2), *Mus musculus* (mouse) Mylpf  
241 (NP\_058034.1), *Oryctolagus cuniculus* (rabbit) Mylpf (NP\_001076230.2), *Gallus gallus*  
242 (chicken) Mylpf (NP\_001185673.1), *Xenopus tropicalis* (frog) Mylpf (CAJ83266.1), *Danio rerio*  
243 (zebrafish) Mylpfa (NP\_571263.1), *Danio rerio* (zebrafish) Mylpfb NP\_001004668.1,  
244 *Callorhinchus milii* (elephant shark) skeletal Myl2 (AFP05921.1), *Eptatretus burgeri* (hagfish)  
245 Myl2 (ENSEBUT00000005213.1), *Todarodes pacificus* (Japanese flying squid) light chain-2  
246 (LC2; P08052), *Chlamys nipponensis akazara* (Japanese bay scallop) myosin light chain  
247 regulatory (MLR; P05963), *Dictyostelium discoideum* (Dicty) RLC (AAA33226.1), and

248 *Saccharomyces cerevisiae* (yeast) Mlc2 (ONH78313.1). The human MYLPP orthologs shown  
249 are regulatory light chain genes MLC2 (NP\_000423.2), MLC5 isoform 1 (NP\_002468.1), MLC7  
250 (AAH27915.1), MLC9 isoform A (NP\_006088.2), MLC10 (ENST00000223167.4), MLC12A  
251 (NP\_001289977.1), and MLC12B (NP\_001138417.1) as well as essential light chains MLC1  
252 (NP\_524144), MLC3 (NP\_524146.1), MLC4 (NP\_001002841.1), MLC6 isoform 1  
253 (NP\_066299.2), and MLC6 isoform 2 (NP\_524147.2). Sequence alignments are ordered by  
254 their similarity to human MYLPP. Expression patterns are described previously.<sup>44-46</sup>

255

## 256 **Results**

### 257 *Identification of variants in MYLPP*

258 Family A, of European ancestry, consisted of two affected siblings born to unaffected parents.  
259 Analysis of high-density genotyping data suggested that the siblings were the products of a  
260 consanguineous mating ( $F=0.0189$ ). This observation was later confirmed by review of pedigree  
261 records that documented the parents were second cousins once-removed. Each affected child,  
262 a male last evaluated at 13 years of age and a female last examined at 24 years of age, had  
263 severe contractures of the hands, fingers, wrists, elbows, hips, knees, ankles, and neck;  
264 pterygia of the elbows and knees; small mouths; and short stature ( $< 1$  percentile for weight and  
265 at  $\sim 1.1$  percentile for height (Table 1). Family B comprised an adopted child of East Indian  
266 ancestry whose parents were predicted to be first cousins based on analysis of high-density  
267 genotyping data ( $F=0.0657$ ) and who was homozygous for the same variant as found in the  
268 siblings in Family A. The proband of Family B, last examined at 6 years of age, also had similar  
269 clinical findings to the siblings in Family A including a small mouth, micrognathia, scoliosis,  
270 contractures of the hands and wrists, and severe right clubfoot that was recalcitrant to  
271 treatment, ultimately leading to amputation of the lower leg. Pathological exam of the foot  
272 revealed complete absence of skeletal muscle that was confirmed histologically (Figure 1). In  
273 both families, we identified homozygosity for a variant (c.470G>T) in a single gene, *myosin light*

274 *chain, phosphorylatable fast skeletal muscle (MYLPF [MIM 617378; Refseq accession number*  
275 *NM\_013292.4])* (Table 1; Figure 2). This variant is predicted to result in p.Cys157Phe  
276 substitution and has a CADD (v1.6) score of 27.5. *MYLPF* had been considered *a priori* to be a  
277 high-priority DA candidate gene because of its role in development of skeletal muscle.<sup>10</sup> Sanger  
278 sequencing validated homozygosity of the c.470G>T variant in all affected persons and that the  
279 parents in Family A were heterozygous carriers. These results suggested that homozygosity for  
280 c.470G>T in *MYLPF* resulted in a pattern of multiple congenital contractures virtually  
281 indistinguishable from that observed in persons with DA, specifically DA1.

282 In an effort to find additional families with a pathogenic variant in *MYLPF* and clinical  
283 characteristics of DA1, we submitted genetic data and phenotypic information to the  
284 MatchMaker Exchange (MME) via the MyGene2 node and identified two additional families (E  
285 and F) that had been submitted to the GeneMatcher node. Simultaneously, we queried  
286 commercial genetic testing companies and colleagues about families in which *MYLPF* had been  
287 identified as a candidate gene. One commercial lab, GeneDx, responded that clinicians for two  
288 families (C and D) had agreed to be contacted by us and provide de-identified genetic and  
289 phenotypic information for review.

290 The proband of Family C was a female, born in Pakistan to unaffected parents, and last  
291 evaluated at 29 years of age. She had short stature, nearsightedness, mild conductive hearing  
292 loss diagnosed in adulthood, scoliosis, bilateral clubfeet, and multiple congenital contractures  
293 including the hands, wrists, elbows, shoulders. ES demonstrated that she was homozygous for  
294 the variant, c.469T>C (p.Cys157Arg) in *MYLPF*, with a CADD score of 25.2. Family D consisted  
295 of an affected stillborn female born to unaffected, first cousin parents from Pakistan. At 35  
296 weeks estimated gestational age a prenatal ultrasound demonstrated polyhydramnios,  
297 shortened long bones, “clenched hands” and bilateral clubfeet. The fetus was subsequently  
298 stillborn and postmortem examination confirmed the prenatal findings. Proband-only ES of the  
299 fetus demonstrated she was also homozygous for the c.469T>C in *MYLPF*. The proband of

300 Family E was a male of Pakistani ancestry, whose parents were first cousins. At ~13 weeks  
301 gestational age, a prenatal ultrasound detected nuchal edema, a septated cystic hygroma, mild  
302 enlarged renal pelvis, and normal amniotic fluid. At 19 weeks gestational age, an ultrasound  
303 showed decreased fetal movements with fetal hypokinesia and akinesia of lower limbs, clubfeet,  
304 thoracic kyphosis and scoliosis, generalized edema (trunk and nuchal) and normal amniotic fluid  
305 volume. He had multiple congenital contractures of the hands, wrists, elbows, shoulders, hips,  
306 knees and bilateral clubfeet as well as pterygia of the neck. He died at one month of age and  
307 was found to be homozygous for the c.469T>C variant in *MYLPP* found in Families C and D.  
308 Both parents were heterozygous.

309 Family F (Table 1 and Figure S1) is a large kindred from South India in which four  
310 individuals were each homozygous for c.470G>T in *MYLPP*. Individuals III-2 and III-3 were the  
311 offspring of a consanguineous mating between II-1 and II-2 whereas individuals III-5 and III-6,  
312 who had two affected fetuses (IV-8 and IV-10), were not known to be closely related but grew  
313 up in the same community. Individual III-3 and both affected fetuses (IV-8 and IV-10) had  
314 contractures of the hands and feet, while III-2 had contractures of only the hands. None of the  
315 heterozygous carriers tested (II-1, II-2, III-5, and III-6) had congenital contractures.

316 Collectively, we identified two unique missense variants affecting the same residue,  
317 p.(Cys157), in *MYLPP* in ten individuals in six unrelated families (A-F) who had been diagnosed  
318 with multiple congenital contractures. Both missense variants are exceedingly rare (maximum  
319 frequency in any super-population in gnomAD = 0.00013 in South Asians for c.470G>T and  
320 0.00009 in Finnish for c.469T>C, and no homozygotes reported) among >151,000 individuals  
321 included in publicly available databases: 1000 Genomes phase 3, the gnomAD browser  
322 (v2.0.2), or UK10K (February 15, 2016 release) and have high Phred-scaled CADD scores,  
323 consistent with pathogenic dominant variants (Table 1). High-density chip genotype data  
324 (Illumina Human Core Exome) was available for one affected individual of East Indian ancestry  
325 (Family B) and one affected individual in the family of Polish ancestry (Family A), both of whom

326 were homozygous for the first variant, c.470G>T. We searched for a shared haplotype that  
327 would provide evidence that this variant is a founder mutation, but their genotypes differed at  
328 even the nearest SNP flanking the variant (both C/C at chr16:30368510 [rs13335932]; both  
329 homozygous for c.470G>T at chr16:30389181; but at chr16:30393147 [rs34518080], the Polish  
330 individual was A/A while the East Indian individual was C/C), leaving at most a short shared  
331 haplotype. Combined with the observation of this variant in multiple populations in gnomAD, it  
332 seems likely that this variant has either arisen independently in different populations or early in  
333 human history. In contrast, the variant shared among all three Pakistani families, c.469T>C,  
334 may be a founder mutation based on their shared ancestry, but we were unable to obtain the  
335 original exome sequence data to confirm the presence of a shared haplotype.

336 In a seventh family (Family G), a one-year-old male proband was found to be  
337 heterozygous for a c.487G>A, p.(Gly163Ser) variant that arose *de novo* in his father. The family  
338 was of Ashkenazi Jewish origin. The proband, last evaluated at 12 months of age, had multiple  
339 congenital contractures including bilateral camptodactyly and overriding fingers, adducted  
340 thumbs, ulnar deviation of the wrists, bilateral hip dislocations, and bilateral vertical talus. He  
341 had a mild kyphosis, bilateral inguinal hernias, small palpebral fissures, epicanthal folds,  
342 anteverted nares with hypoplastic alae nasae, long philtral folds, a thin upper lip, small mouth,  
343 high-arched palate without cleft, and micro-retrognathia. Because of recurrent apnea, he  
344 underwent a tracheostomy. His father had similar facial features, ulnar deviation of the hands,  
345 and had undergone multiple corrective procedures for contractures of the ankles. Manual review  
346 in IGV of the proband's exome sequence data did not reveal any additional rare variants in  
347 *MYLPP* and no candidate variants were found in other genes known to underlie DA. Depth of  
348 sequencing of all exons of these genes was >10X and there was no evidence of a copy number  
349 variant that would explain his features. This variant had a CADD score of 32.0.

350 Family H is a family in which the two probands, individuals IV-1 and IV-3, were  
351 independently diagnosed with distal arthrogyriposis (DA). Individual IV-3 was first evaluated at 7

352 months of age because of a bilateral ulnar finger deviation, flexed thumbs, right calcaneovalgus  
353 deformity and left clubfoot. Several months later, her cousin (IV-1) was referred to an  
354 arthrogyposis clinic for evaluation of bilateral ulnar deviation and bilateral clubfoot (Figure 1).  
355 The mother and grandmother of each proband also had congenital contractures (Table 1).  
356 Individual IV-3, last evaluated at 6 years of age, has no growth retardation or scoliosis, neither  
357 her mother nor grand-mother. Clinical exome sequencing of IV-3 and III-2 revealed  
358 heterozygosity for a c.98C>T p.(Ala33Val) (NM\_013292) and Sanger sequencing confirmed it  
359 was present in III-6 and II-7 (Table 1 and Supplementary Figure 1). This variant is predicted to  
360 be damaging with a CADD score of 31.0 and is absent from gnomAD v2.1.1; accessed on  
361 04/12/2020. Dominant inheritance of DA in Families G and H suggest that p.(Gly163Ser) and  
362 p.(Ala33Val) may impact MYLPF function more severely than the recessive variants,  
363 p.(Cys157Phe) and p.(Cys157Ser).

364

### 365 *Loss of zebrafish mylpf function causes muscle weakness and loss*

366 Mylpf structure is highly conserved among vertebrates suggesting that function is also  
367 conserved. Previous studies showed that mice homozygous for a null *mylpf* allele lack all  
368 skeletal muscle at birth.<sup>10</sup> However, these studies did not determine whether muscle failed to  
369 develop or underwent degeneration after normal development, nor did they explain how  
370 complete or partial loss of function of MYLPF function in humans selectively and/or  
371 disproportionately affects muscles of the limb. To generate a vertebrate model for partial loss of  
372 function, we knocked out zebrafish *mylpfa*, one of the two zebrafish *Mylpf* orthologs. Both  
373 orthologs, *mylpfa* and *mylpfb*, are expressed specifically in embryonic and larval fast-twitch  
374 myofibers,<sup>47</sup> with *mylpfa* being the predominantly expressed gene (Figure 3A-E). We used  
375 CRISPR/Cas9-mediated mutagenesis to generate two independent *mylpfa* alleles, *mylpfa*<sup>oz30</sup>  
376 and *mylpfa*<sup>oz43</sup> (Figure 3F). Both alleles frameshift the protein within the first of two EF-hand

377 domains (Figure 3G, H) and are thus predicted to be nulls. However, homozygous *mylpfa*  
378 mutant embryos are expected to retain some Mylpf function because they still have a functional  
379 *mylpfb* gene.

380 Pectoral fins of the *mylpfa* mutant are completely paralyzed, and the mutant has an  
381 impaired escape response (Figure 3I, J, Movies S1 and S2). To directly measure contractile  
382 strength of trunk muscle, we electrically stimulated live intact 3 dpf embryos mounted between a  
383 hook at the head and a force transducer at the tail. At all frequencies tested, *mylpfa*<sup>oz30</sup>  
384 homozygous mutant embryos are significantly weaker than their unaffected siblings (P<0.001 at  
385 20 Hz and 180 Hz) (Figure 3K). To characterize the motion-generating capacity of myosin with  
386 their constituent light chains, we extracted monomeric myosin from *mylpfa* mutant and sibling  
387 wild-type fish onto the surface of a microscope flow cell chamber (see Methods). Fluorescent,  
388 filamentous actin was introduced into the chamber and actin motion generated by the extracted  
389 myosin was imaged. We observed that the actin filament velocity was significantly slower in  
390 both *mylpfa*<sup>oz30</sup> and *mylpfa*<sup>oz43</sup> compared to wild-type siblings (Figure 3L, M, Movie S3). The  
391 remaining and apparently compromised myosin motile function and contractile force observed  
392 could be due to residual *mylpf* function in fast-twitch muscles (provided by *mylpfb*) and/or intact  
393 slow-twitch muscles, which do not express *mylpfa* and appear normal (Figures 3A-D and 4C-F).  
394 Thus, like persons with DA, zebrafish *mylpfa* mutants display abnormal movement that is more  
395 pronounced in limbs; this weakness can be explained at least in part by impaired myosin force  
396 and motion generation in fast-twitch muscle.

397 We next examined zebrafish muscle over time, to learn whether *mylpfa* mutant muscles  
398 form and then deteriorate or whether they fail to develop in the first place. This distinction may  
399 be particularly important for understanding the complete absence of skeletal muscle that was  
400 observed in the foot of one child with DA associated with a p.(Cys157Phe variant). Shortly after  
401 somite formation, *mylpfa* mutant muscle morphology appears normal (Figure 4A, B). However,  
402 at 6 days post fertilization (dpf), *mylpfa* mutant myotomes are significantly (p<0.05) reduced in



403 dorsal-ventral height compared to wild-type (WT = 266  $\mu\text{m}$ , N = 12; *mylpfa*<sup>-/-</sup>=232  $\mu\text{m}$ , N=6) and  
404 muscle fibers are irregularly shaped, suggesting that fast-twitch fibers deteriorate over time  
405 (Figure 4C, D). Slow-twitch muscle fibers are spared in the same fish (Figure 4E, F). Muscle  
406 defects are most pronounced in a specific appendicular muscle, the posterior hypaxial muscle  
407 (PHM) (Figure 4G-J). Although the PHM forms at the normal time in *mylpfa* mutants and is  
408 initially comprised of multinucleate muscle, the muscle fibers break down into small 'islands' that  
409 are often mononucleate by 4 dpf (Figure 4I, J). Muscle deterioration in the PHM is especially  
410 rapid compared to axial muscle, since axial muscle fibers form prior to appendicular fibers, yet  
411 are still relatively intact and multinucleate at 6 dpf (compare Figure 4D and J insets).

412 To examine whether *mylpfa* mutant PHM cellular 'islands' are degenerated fibers or  
413 newly forming mononucleate myoblasts, we conducted confocal time-lapse microscopy  
414 beginning at 84 hpf (Figure 4K-M; Movie S4). At time-lapse outset, most PHM fibers are intact,  
415 with wavy membranes that occasionally are narrowed almost to closure (Figure 4K, L).  
416 Membrane irregularities become more pronounced over time, and pieces of fiber pinch off  
417 (Figure 4L, M). During each time-lapse (N=3), a new PHM fiber was added (Figure 4L, M),  
418 suggesting that hyperplastic growth continued during the imaging period. Together, these  
419 findings indicate that zebrafish *mylpfa* is required to maintain myofiber integrity but is not  
420 required for initial myofiber formation or hyperplastic growth. Accordingly, we hypothesize that  
421 the segmental amyoplasia in individuals with pathogenic variants results myofibers that form  
422 normally but subsequently degenerate.

423

#### 424 *Protein modelling of MYLPF variants*

425 To better understand how MYLPF p.(Cys157Phe) and p.(Cys157Arg) variants versus  
426 the p.(Ala33Val) and p.(Gly163Ser) variants underlie recessive versus dominantly inherited DA,  
427 respectively, we examined a previously developed protein model of the rabbit Mylpf-MyI1-  
428 Myosin heavy chain-Actin complex (PBD 5H53)<sup>43</sup> (Figure 5A, B). Rabbit Mylpf protein is shifted

429 one amino acid relative to the corresponding residues in the human counterparts (Figure 5C)  
430 but for simplicity, we refer to equivalent MYLPP/Mylpf residues using human numbering across  
431 species. Ala33 is conserved in all eukaryotes examined, Gly163 is deeply conserved from  
432 scallop to human, but Cys157 is conserved only among vertebrates (Figure 5C). The protein  
433 model reveals that Ala33 is positioned adjacent to the myosin heavy chain and Mylpf Gly163  
434 directly contacts a phenylalanine near the hook region of myosin heavy chain (Figure 5A). In  
435 contrast, Mylpf Cys157 is buried deep within the regulatory light chain and makes no contact  
436 with myosin heavy chain (Figure 5A).

437 To determine whether the interaction between Mylpf Gly163 and myosin heavy chain is  
438 conserved, we compared crystal structures of scallop, squid and chicken myosin light and heavy  
439 chains to the rabbit structure (Figure 5D-G; structures generated in<sup>39-42</sup>). In chicken, as in  
440 rabbit, Gly163 directly contacts a phenylalanine residue in the heavy chain (Figure 5F, G).  
441 Gly163 is found on the surface of the RLC in scallop and positioned very close the myosin  
442 heavy chain in squid (Figure 5D, E). Because Gly163 is present in animals that diverged from  
443 vertebrates prior to regulatory light chain gene family diversification, we reasoned that MYLPP  
444 orthologs may also contain this residue. Alignment of human MYLPP orthologs reveals perfect  
445 conservation of glycine in the position corresponding to human Gly163. Some essential light  
446 chain proteins also have a corresponding glycine, suggesting that it arose very early in light  
447 chain gene evolution (Figure 5H). Likewise, Ala33 is conserved in all light chains examined  
448 including both ELCs and RLCs and is positioned close to the heavy chain in the crystal  
449 structures examined (Figure 5C-H). In contrast, only three of the eight human regulatory light  
450 chain genes contain a cysteine in the Cys157 position (Figure 5H), revealing that although  
451 Cys157 is conserved among vertebrate Mylpf genes (Figure 5C), some orthologous regulatory  
452 light chain genes have a different residue in this position. Together these findings indicate that  
453 Ala33 arose prior to animal evolution, Gly163 arose early in animal evolution, and these  
454 residues directly or almost-directly contact the myosin heavy chain in vertebrates. These

455 observations suggest that the *MYLPF* p.(Ala33Val) and p.(Gly163Ser) variants have dominant  
456 effects because they more directly impact interactions with myosin heavy chain than the Cys157  
457 variants.

458

## 459 **Discussion**

460 We identified four pathogenic variants in *MYLPF* in eight unrelated families in which  
461 seventeen affected individuals share similar phenotypic features, suggesting that mutations in  
462 *MYLPF* underlie a previously unrecognized multiple malformation syndrome. This condition is  
463 characterized by multiple congenital contractures, scoliosis, and short stature and is clinically  
464 indistinguishable from DA1 due to mutations in genes encoding other components of the  
465 contractile apparatus (e.g., embryonic myosin, troponins, tropomyosin). However, we find that  
466 short stature and proximal joint contractures (i.e., elbows, hips, knees) appear more commonly  
467 in DA1 due to variants in *MYLPF* than in DA1 due to other variants in other genes (*MYH3*,  
468 *TNNI2*, *TNNT3* and *TPM2*).<sup>5,6</sup> Nevertheless, because the number of families with pathogenic  
469 variants reported is small, the extent of overlap between their phenotypic features and those of  
470 individuals with variants in *MYH3*, *TNNI2*, *TPM2* and *TNNT3* remains to be determined.

471 In contrast to the clinical findings of DA1 specifically, and of DAs in general, a single  
472 individual had segmental amyoplasia of the foot with fatty replacement of the muscle. We did  
473 not observe this finding in other persons with DA due to *MYLPF* variants, but we lacked  
474 pathological or imaging data of the limbs for all but one additional case, an affected fetus that  
475 underwent post-mortem exam at 19 weeks. Whether this is a finding in other individuals with  
476 pathogenic variants in *MYLPF* is unclear. To our knowledge, complete absence of limb skeletal  
477 muscles in a person with DA has not been reported. Hypoplasia or aplasia of the muscles of the  
478 upper and / or lower limbs is the defining feature of a group of arthrogyposis conditions known  
479 as Amyoplasia.

480 Amyoplasia is the most common condition referred to as arthrogyriposis, accounting for  
481 ~30% of all persons diagnosed with arthrogyriposis.<sup>48</sup> The etiology is suspected to be  
482 heterogeneous (i.e., vascular disruption, monogenic, somatic mosaicism, oligogenic, etc.) and  
483 the heritability of Amyoplasia, if any, remains unknown. The overwhelming majority of cases of  
484 Amyoplasia are simplex, but rare instances of affected siblings have been reported. In such  
485 cases, amyoplasia is typically limited to either the upper or lower limbs.<sup>49</sup> In a small subset of  
486 such families with lower limb amyoplasia (LLA), pathogenic variants have been found in one of  
487 several genes including *BICD2*,<sup>50</sup> *CACNA1H*,<sup>51</sup> *DYNC1H1*,<sup>52</sup> *TRPV4*,<sup>53</sup> and *FKBP10*.<sup>54</sup> In each  
488 of the LLA conditions resulting from pathogenic variants in these genes, neurological  
489 abnormalities including weakness and hypotonia are typically present, distinguishing them from  
490 DA1 due to *MYLPF* variants. However, absence or severe atrophy of select muscles of the  
491 lower limbs is also common, if not typical, in these conditions, suggesting segmental amyoplasia  
492 is a genetically heterogeneous trait. Moreover, these observations suggest that, at least in some  
493 families with Amyoplasia, large effect risk allele(s) might be segregating.

494 Our findings indicate that DA1 due to pathogenic variants in *MYLPF* can be transmitted  
495 as either an autosomal dominant or autosomal recessive condition. Nearly 400 genes  
496 underlying Mendelian conditions transmitted in both dominant and recessive inheritance  
497 patterns have been reported (J.X. Chong et al., 2019, Am. Soc. Hum. Genet., abstract). In the  
498 majority of these instances, the resulting Mendelian conditions have overlapping but different  
499 phenotypic features suggesting that while the inheritance patterns may differ, the pathogenesis  
500 for each is similar. In some cases, including DA1 due to variants in *MYLPF*, the clinical  
501 characteristics of the dominant and recessive conditions are virtually indistinguishable (e.g.,  
502 cataracts due to variants in *CRYAA*). Differences in inheritance patterns can result from a  
503 variety of phenomena, including variants that affect distinct functional domains, result in loss

504 versus gain-of-function, affect different tissue-specific transcripts, and have dose-dependent  
505 effects on gene function.

506           Substitutions of Gly163 and Ala33 in MYLPF both result in dominant DA1 whereas  
507 substitution of Cys157 underlies recessive DA1. These three residues are each conserved  
508 among all vertebrate MYLPF homologs, but Ala33 and Gly163 are more deeply conserved than  
509 Cys157. Indeed, Ala33 is found in all light chain genes examined and Gly163 is found in all  
510 animal RLC genes reviewed. This broad conservation suggests that Ala33 and Gly163 are vital  
511 to RLC identity. These two residues sit on the surface of MYLPF that contacts MyHC, whereas  
512 Cys157 is buried within MYLPF. This indicates that Ala33 and Gly163 might directly participate  
513 in critical protein-protein interactions. Perturbation of these residues may directly affect the  
514 packing of MyHC molecules into the thick filament, which might in turn alter the function of other  
515 nearby myosins in this multimeric structure. Disruption of MYLPF amino acid residues that are  
516 positioned further from MyHC (e.g., Cys157) may result in lesser adverse effects on force  
517 transduction.

518           Based on the rabbit crystal structure, Ala33 and Gly163 may contact residues in human  
519 embryonic myosin, MYH3, that are affected in other DA conditions. Specifically, Gly163 is  
520 predicted to directly contact a phenylalanine residue in the MyHC that corresponds to Phe835 in  
521 MYH3. We previously reported an alteration at this MYH3 residue (c.2503\_2505delTTC;  
522 p.(Phe835del)) in an individual with DA2A, the most severe of DA conditions. Similarly, Ala33 is  
523 positioned directly adjacent to a residue in MyHC that corresponds to MYH3 Lys838, a residue  
524 that we previously reported to be altered (c.2512A>G; p.(Lys838Glu)) in an individual with  
525 DA2B. In both cases, the condition (DA1) resulting from perturbation of MYLPF is less severe  
526 than the conditions (DA2A and DA2B) due to altering corresponding residues in MYH3. This  
527 difference in disease severity may reflect differences in protein function as MYLPF is thought to  
528 act primarily by stabilizing MyHC structure.<sup>7,55</sup> We predict that other deeply conserved MYLPF

529 residues that are positioned adjacent to disease-associated MyHC residues, such as MYLPPF  
530 residues Glu29 and Glu32, may, if altered, also lead to dominantly inherited DA1.

531 We showed that myosin extracted from *mylpfa*-deficient zebrafish moves actin filaments  
532 more slowly than wild-type myosin extracts. The slowing (~75% of full speed) is less  
533 pronounced than was found in previous studies which removed myosin RLCs *in vitro* (~33% of  
534 full speed)<sup>8,9</sup> and compared to *in vitro* extracted chicken myosin bearing a point mutation in  
535 Mylpf p.(Phe102Leu) (~50% of full speed).<sup>56</sup> We speculate that the effect of *mylpfa* loss is  
536 milder than was seen in these previous assays because the mutant still has some RLC function,  
537 provided by *mylpfb* in fast fibers and by a normal set of RLCs in slow-twitch fibers. While the  
538 effect on actin motility is modest, total trunk muscle force is dramatically decreased in *mylpfa*  
539 mutants and the pectoral fins are completely paralyzed. This parallels the phenotypic  
540 consequences observed in DA1, and DAs in general, in which the more distal body areas (e.g.,  
541 hands vs. shoulders) are more frequently and more severely affected.

542 In addition to muscle weakness and pectoral fin paralysis, zebrafish *mylpfa* mutant  
543 muscle fibers eventually degenerate in all muscles, with the PHM being most severely affected.  
544 This degeneration indicates that Mylpf function is essential for muscle integrity during early  
545 development and suggests mechanisms for muscle loss in humans with DA1. *Mylpfa* is a  
546 marker of fast-twitch myofibers and is abundantly expressed in PHM whereas there are few  
547 *smyh2*-positive slow twitch fibers and no *smyh1*-positive slow-twitch fibers in the PHM  
548 suggesting that it is composed largely of fast-twitch myofibers.<sup>23,30,57</sup> In contrast, slow-twitch  
549 myofibers are more common in myotomes where they may exert a stabilizing effect. Our finding  
550 that the PHM is most strongly affected is consistent with the observation that the most severe  
551 contractures in DA1, as well as muscle hypoplasia and/or aplasia, occur more frequently in the  
552 most distal regions of the limb (e.g., digits, hands, wrists, feet, and ankles). Muscle fibers in  
553 myotomes also become irregularly shaped over time in *mylpfa* knockouts, consistent with the

554 observation that the trunk muscles of persons with DA1 due to *MYLPF* variants are typically  
555 affected but more mildly than the limbs.

556 In summary, we discovered that variants in *MYLPF* underlie both dominant and  
557 recessive forms of a distal arthrogyrosis with features typically seen in DA1. The distribution of  
558 these features in persons with DA1 due to *MYLPF* variants largely overlaps that of DA1 due to  
559 variants in *MYH3*, *TNNI2*, *TPM2*, and *TNNT3*, with proximal joint contractures perhaps more  
560 common in individuals with *MYLPF* variants. However, segmental amyoplasia appears to be a  
561 unique feature of DA1 due to *MYLPF* that, based on knockout of *mylpfa* in zebrafish, results  
562 from degeneration of differentiated skeletal myofibers.

563

#### 564 **Supplemental Materials and Methods**

565 Supplemental information includes one figure (S1), four movies (S1-S4), and supplemental  
566 methods.

567

#### 568 **Acknowledgements**

569 We thank the families for their participation and support. Sequencing was provided by the  
570 University of Washington Center for Mendelian Genomics (UW-CMG) and was funded by  
571 NHGRI and NHLBI grants UM1 HG006493 and U24 HG008956, by the Office of the Director,  
572 NIH under Award Number S10OD021553, and by the National Institute of Child Health and  
573 Human Development (1R01HD048895 to M.J.B.). We thank the Ohio State Rightmire Hall  
574 zebrafish staff for excellent animal care and husbandry and Mark Nilan and Mika Gallati for  
575 zebrafish care and mutant identification at the University of Maine. We thank Sarah Shepherd  
576 for assistance during initial *mylpfa*<sup>oz43</sup> construction. Zebrafish work was funded by NIH grants  
577 GM088041 and GM117964 (to S.L.A.), an NIH T32 training grant NS077984 and an Ohio State  
578 Pelotonia postdoctoral fellowship (to J.C.T.), Ohio State Edward Mayers and Elizabeth Wagner  
579 research scholarships (to E.M.T), and HL150953 and AR067279 (to D.M.W.). The Ohio State

580 Neuroscience Imaging Core facilities are supported by NIH grants P30-NS045758, P30-  
581 NS104177 and S10-OD010383. We acknowledge the DNA Sequencing Shared Resource at  
582 The Ohio State University Comprehensive Cancer Center. This work was also supported by the  
583 Indian Council of Medical Research, Government of India (No.5/13/58/2015/NCD-III). The F310  
584 antibody developed by Frank Stockdale was obtained from the Developmental Studies  
585 Hybridoma Bank, created by the NICHD of the NIH and maintained at The University of Iowa,  
586 Department of Biology. The authors are grateful to Mrs Séverine Drouhin and to the Molecular  
587 Biology Facility of the Grenoble University Hospital, France for technical assistance. The  
588 content is solely the responsibility of the authors and does not necessarily represent the official  
589 views of the National Institutes of Health.

590

591

592

### 593 **Web resources**

594 The URLs for data presented herein are as follows:

595 Geno2MP: <https://geno2mp.gs.washington.edu/Geno2MP/>

596 gnomAD: <http://gnomad.broadinstitute.org>

597 Human Genome Variation: <http://www.hgvs.org/mutnomen/>

598 Online Mendelian Inheritance in Man (OMIM): <http://www.omim.org/>

599 PDB: <http://www.rcsb.org/>

600 EMBL-EBI expression atlas: <https://www.ebi.ac.uk/gxa/home>

601

### 602 **References**

603

604 1. Bamshad, M., Jorde, L.B., and Carey, J.C. (1996). A revised and extended classification of  
605 the distal arthrogyposes. *Am J Med Genet* 65, 277–281.



- 606 2. Bamshad, M., Bohnsack, J.F., Jorde, L.B., and Carey, J.C. (1996). Distal arthrogyriposis type  
607 1: Clinical analysis of a large kindred. *Am J Med Genet* 65, 282–285.
- 608 3. Stevenson, D.A., Carey, J.C., Palumbos, J., Rutherford, A., Dolcourt, J., and Bamshad, M.J.  
609 (2006). Clinical Characteristics and Natural History of Freeman-Sheldon Syndrome. *Pediatrics*  
610 117, 754–762.
- 611 4. Krakowiak, P.A., Bohnsack, J.F., Carey, J.C., and Bamshad, M. (1998). Clinical analysis of a  
612 variant of Freeman-Sheldon syndrome (DA2B). *Am J Med Genet* 76, 93–98.
- 613 5. Beck, A.E., McMillin, M.J., Gildersleeve, H.I.S., Shively, K.M.B., Tang, A., and Bamshad, M.J.  
614 (2014). Genotype-phenotype relationships in Freeman–Sheldon syndrome. *Am J Med Genet A*  
615 164, 2808–2813.
- 616 6. Toydemir, R.M., Rutherford, A., Whitby, F.G., Jorde, L.B., Carey, J.C., and Bamshad, M.J.  
617 (2006). Mutations in embryonic myosin heavy chain (MYH3) cause Freeman-Sheldon syndrome  
618 and Sheldon-Hall syndrome. *Nat Genet* 38, 561–565.
- 619 7. Lowey, S., and Trybus, K.M. (2010). Common structural motifs for the regulation of divergent  
620 class II myosins. *J Biological Chem* 285, 16403–16407.
- 621 8. Lowey, S., Waller, G.S., and Trybus, K.M. (1993). Skeletal muscle myosin light chains are  
622 essential for physiological speeds of shortening. *Nature* 365, 454–456.
- 623 9. VanBuren, P., Waller, G.S., Harris, D.E., Trybus, K.M., Warshaw, D.M., and Lowey, S.  
624 (1994). The essential light chain is required for full force production by skeletal muscle myosin.  
625 *Proc National Acad Sci* 91, 12403–12407.
- 626 10. Wang, Y., Szczesna-Cordary, D., Craig, R., Diaz-Perez, Z., Guzman, G., Miller, T., and  
627 Potter, J.D. (2007). Fast skeletal muscle regulatory light chain is required for fast and slow  
628 skeletal muscle development. *Faseb J* 21, 2205–2214.
- 629 11. Goody, M.F., Carter, E.V., Kilroy, E.A., Maves, L., and Henry, C.A. (2016). “Muscling”  
630 Throughout Life: Integrating Studies of Muscle Development, Homeostasis, and Disease in  
631 Zebrafish. *Curr Top Dev Biol* 124, 197–234.
- 632 12. Jackson, H.E., and Ingham, P.W. (2013). Control of muscle fibre-type diversity during  
633 embryonic development: The zebrafish paradigm. *Mech Develop* 130, 447–457.
- 634 13. Li, M., Hromowyk, K.J., Amacher, S.L., and Currie, P.D. (2016). Muscular dystrophy  
635 modeling in zebrafish. *Methods Cell Biol* 138, 347–380.
- 636 14. Talbot, J., and Maves, L. (2016). Skeletal muscle fiber type: using insights from muscle  
637 developmental biology to dissect targets for susceptibility and resistance to muscle disease.  
638 *Wiley Interdiscip Rev Dev Biology* 5, 518–534.
- 639 15. Bird, N.C., Windner, S.E., and Devoto, S.H. (2011). *Methods in Molecular Biology*. *Methods*  
640 *Mol Biology Clifton N J* 798, 153–169.

- 641 16. Devoto, S.H., Melançon, E., Eisen, J.S., and Westerfield, M. (1996). Identification of  
642 separate slow and fast muscle precursor cells in vivo, prior to somite formation. *Dev Camb Engl*  
643 *122*, 3371–3380.
- 644 17. Kimmel, C.B., Ballard, W.W., Kimmel, S.R., Ullmann, B., and Schilling, T.F. (1995). Stages  
645 of embryonic development of the zebrafish. *Dev Dynam* *203*, 253–310.
- 646 18. Xu, Y., He, J., Wang, X., Lim, T.M., and Gong, Z. (2000). Asynchronous activation of 10  
647 muscle-specific protein (MSP) genes during zebrafish somitogenesis. *Dev Dynam* *219*, 201–  
648 215.
- 649 19. Haines, L., Neyt, C., Gautier, P., Keenan, D.G., Bryson-Richardson, R.J., Hollway, G.E.,  
650 Cole, N.J., and Currie, P.D. (2004). Met and Hgf signaling controls hypaxial muscle and lateral  
651 line development in the zebrafish. *Development* *131*, 4857–4869.
- 652 20. Masselink, W., Cole, N.J., Fenyés, F., Berger, S., Sonntag, C., Wood, A., Nguyen, P.D.,  
653 Cohen, N., Knopf, F., Weidinger, G., et al. (2016). A somitic contribution to the apical  
654 ectodermal ridge is essential for fin formation. *Nature* *535*, 542–546.
- 655 21. Minchin, J.E.N., Williams, V.C., Hinitz, Y., Low, S., Tandon, P., Fan, C.-M., Rawls, J.F., and  
656 Hughes, S.M. (2013). Oesophageal and sternohyal muscle fibres are novel Pax3-dependent  
657 migratory somite derivatives essential for ingestion. *Dev Camb Engl* *140*, 2972–2984.
- 658 22. Neyt, C., Jagla, K., Thisse, C., Thisse, B., Haines, L., and Currie, P.D. (2000). Evolutionary  
659 origins of vertebrate appendicular muscle. *Nature* *408*, 82–86.
- 660 23. Talbot, J.C., Teets, E.M., Ratnayake, D., Duy, P.Q., Currie, P.D., and Amacher, S.L. (2019).  
661 Muscle precursor cell movements in zebrafish are dynamic and require Six family genes. *Dev*  
662 *Camb Engl* *146*, dev171421.
- 663 24. Chong, J.X., Buckingham, K.J., Jhangiani, S.N., Boehm, C., Sobreira, N., Smith, J.D.,  
664 Harrell, T.M., McMillin, M.J., Wiszniewski, W., Gambin, T., et al. (2015). The Genetic Basis of  
665 Mendelian Phenotypes: Discoveries, Challenges, and Opportunities. *Am J Hum Genetics* *97*,  
666 199–215.
- 667 25. McLaren, W., Gil, L., Hunt, S.E., Riat, H.S., Ritchie, G.R.S., Thormann, A., Flicek, P., and  
668 Cunningham, F. (2016). The Ensembl Variant Effect Predictor. *Biorxiv* 042374.
- 669 26. Paila, U., Chapman, B.A., Kirchner, R., and Quinlan, A.R. (2013). GEMINI: integrative  
670 exploration of genetic variation and genome annotations. *Plos Comput Biol* *9*, e1003153.
- 671 27. Westerfield (2007). *The Zebrafish Book: A guide for the laboratory use of zebrafish (Danio*  
672 *rerio)*.
- 673 28. Ignatius, M.S., Chen, E., Elpek, N.M., Fuller, A.Z., Tenente, I.M., Clagg, R., Liu, S.,  
674 Blackburn, J.S., Lnardic, C.M., Rosenberg, A.E., et al. (2012). In vivo imaging of tumor-  
675 propagating cells, regional tumor heterogeneity, and dynamic cell movements in embryonal  
676 rhabdomyosarcoma. *Cancer Cell* *21*, 680–693.

- 677 29. Tang, Q., Moore, J.C., Ignatius, M.S., Tenente, I.M., Hayes, M.N., Garcia, E.G., Yordán,  
678 N.T., Bourque, C., He, S., Blackburn, J.S., et al. (2016). Imaging tumour cell heterogeneity  
679 following cell transplantation into optically clear immune-deficient zebrafish. *Nat Commun* 7,  
680 10358.
- 681 30. Elworthy, S., Hargrave, M., Knight, R., Mebus, K., and Ingham, P.W. (2008). Expression of  
682 multiple slow myosin heavy chain genes reveals a diversity of zebrafish slow twitch muscle  
683 fibres with differing requirements for Hedgehog and Prdm1 activity. *Dev Camb Engl* 135, 2115–  
684 2126.
- 685 31. Hromowyk, K.J., Talbot, J.C., Martin, B.L., Janssen, P.M.L., and Amacher, S.L. (2020). Cell  
686 fusion is differentially regulated in zebrafish post-embryonic slow and fast muscle. *Dev Biol.* in  
687 press.
- 688 32. Talbot, J.C., and Amacher, S.L. (2014). A streamlined CRISPR pipeline to reliably generate  
689 zebrafish frameshifting alleles. *Zebrafish* 11, 583–585.
- 690 33. Berberoglu, M.A., Gallagher, T.L., Morrow, Z.T., Talbot, J.C., Hromowyk, K.J., Tenente, I.M.,  
691 Langenau, D.M., and Amacher, S.L. (2017). Satellite-like cells contribute to pax7 -dependent  
692 skeletal muscle repair in adult zebrafish. *Dev Biol* 424, 162–180.
- 693 34. Jowett, T. (1999). Analysis of protein and gene expression. *Methods Cell Biol* 59, 63–85.
- 694 35. Martin, B.L., Gallagher, T.L., Rastogi, N., Davis, J.P., Beattie, C.E., Amacher, S.L., and  
695 Janssen, P.M.L. (2015). In vivo assessment of contractile strength distinguishes differential  
696 gene function in skeletal muscle of zebrafish larvae. *J Appl Physiology Bethesda Md* 119,  
697 799–806.
- 698 36. Smith, L.L., Beggs, A.H., and Gupta, V.A. (2013). Analysis of skeletal muscle defects in  
699 larval zebrafish by birefringence and touch-evoked escape response assays. *J Vis Exp Jove*  
700 e50925.
- 701 37. Warshaw, D.M., Desrosiers, J.M., Work, S.S., and Trybus, K.M. (1990). Smooth muscle  
702 myosin cross-bridge interactions modulate actin filament sliding velocity in vitro. *J Cell Biology*  
703 111, 453–463.
- 704 38. Palmiter, K.A., Tyska, M.J., Haeberle, J.R., Alpert, N.R., Fananapazir, L., and Warshaw,  
705 D.M. (2000). R403Q and L908V mutant  $\beta$ -cardiac myosin from patients with familial  
706 hypertrophic cardiomyopathy exhibit enhanced mechanical performance at the single molecule  
707 level. *J Muscle Res Cell M* 21, 609–620.
- 708 39. Li, A., Nelson, S.R., Rahmanseresht, S., Braet, F., Cornachione, A.S., Previs, S.B., O’Leary,  
709 T.S., McNamara, J.W., Rassier, D.E., Sadayappan, S., et al. (2019). Skeletal MyBP-C isoforms  
710 tune the molecular contractility of divergent skeletal muscle systems. *Proc National Acad Sci*  
711 116, 21882–21892.
- 712 40. Himmel, D.M., Gourinath, S., Reshetnikova, L., Shen, Y., Szent-Gyorgyi, A.G., and Cohen,  
713 C. (2002). Crystallographic findings on the internally uncoupled and near-rigor states of myosin:  
714 Further insights into the mechanics of the motor. *Proc National Acad Sci* 99, 12645–12650.

- 715 41. Yang, Y., Gourinath, S., Kovács, M., Nyitray, L., Reutzel, R., Himmel, D.M., O'Neill-  
716 Hennessey, E., Reshetnikova, L., Szent-Györgyi, A.G., Brown, J.H., et al. (2007). Rigor-like  
717 Structures from Muscle Myosins Reveal Key Mechanical Elements in the Transduction  
718 Pathways of This Allosteric Motor. *Structure* 15, 553–564.
- 719 42. Wu, S., Liu, J., Reedy, M.C., Tregear, R.T., Winkler, H., Franzini-Armstrong, C., Sasaki, H.,  
720 Lucaveche, C., Goldman, Y.E., Reedy, M.K., et al. (2010). Electron tomography of cryofixed,  
721 isometrically contracting insect flight muscle reveals novel actin-myosin interactions. *Plos One*  
722 5, e12643.
- 723 43. Fujii, T., and Namba, K. (2017). Structure of actomyosin rigour complex at 5.2 Å resolution  
724 and insights into the ATPase cycle mechanism. *Nat Commun* 8, 13969.
- 725 44. Heissler, S.M., and Sellers, J.R. (2014). Myosin light chains: Teaching old dogs new tricks.  
726 *Bioarchitecture* 4, 169–188.
- 727 45. Reiser, P.J. (2019). Current understanding of conventional and novel co-expression patterns  
728 of mammalian sarcomeric myosin heavy chains and light chains. *Arch Biochem Biophys* 662,  
729 129–133.
- 730 46. Sitbon, Y.H., Yadav, S., Kazmierczak, K., and Szczesna-Cordary, D. (2019). Insights into  
731 myosin regulatory and essential light chains: a focus on their roles in cardiac and skeletal  
732 muscle function, development and disease. *J Muscle Res Cell M* 1–15.
- 733 47. Wagner, D.E., Weinreb, C., Collins, Z.M., Briggs, J.A., Megason, S.G., and Klein, A.M.  
734 (2018). Single-cell mapping of gene expression landscapes and lineage in the zebrafish  
735 embryo. *Science* 360, 981–987.
- 736 48. Hall, J.G., Aldinger, K.A., and Tanaka, K.I. (2014). Amyoplasia revisited. *Am J Med Genet A*  
737 164, 700–730.
- 738 49. Hall, J.G. (2014). Amyoplasia involving only the upper limbs or only involving the lower limbs  
739 with review of the relevant differential diagnoses. *Am J Med Genet A* 164, 859–873.
- 740 50. Frasquet, M., Camacho, A., Vílchez, R., Argente-Escrig, H., Millet, E., Vázquez-Costa, J.F.,  
741 Silla, R., Sánchez-Monteagudo, A., Vílchez, J.J., Espinós, C., et al. (2020). The clinical  
742 spectrum of BICD2 mutations. *Eur J Neurol*.
- 743 51. Carter, M.T., McMillan, H.J., Tomin, A., and Weiss, N. (2019). Compound heterozygous  
744 CACNA1H mutations associated with severe congenital amyotrophy. *Channels* 13, 153–161.
- 745 52. Scoto, M., Rossor, A.M., Harms, M.B., Cirak, S., Calissano, M., Robb, S., Manzur, A.Y.,  
746 Arroyo, A.M., Sanz, A.R., Mansour, S., et al. (2015). Novel mutations expand the clinical  
747 spectrum of DYNC1H1-associated spinal muscular atrophy. *Neurology* 84, 668–679.
- 748 53. Velilla, J., Marchetti, M.M., Toth-Petroczy, A., Grosogoeat, C., Bennett, A.H., Carmichael,  
749 N., Estrella, E., Darras, B.T., Frank, N.Y., Krier, J., et al. (2019). Homozygous TRPV4 mutation  
750 causes congenital distal spinal muscular atrophy and arthrogryposis. *Neurology Genetics* 5,  
751 e312.

- 752 54. Barnes, A.M., Duncan, G., Weis, M., Paton, W., Cabral, W.A., Mertz, E.L., Makareeva, E.,  
753 Gambello, M.J., Lacbawan, F.L., Leikin, S., et al. (2013). Kuskokwim Syndrome, a Recessive  
754 Congenital Contracture Disorder, Extends the Phenotype of FKBP10 Mutations. *Hum Mutat* **34**,  
755 1279–1288.
- 756 55. Pastra-Landis, S.C., and Lowey, S. (1986). Myosin subunit interactions. Properties of the  
757 19,000-dalton light chain-deficient myosin. *J Biological Chem* **261**, 14811–14816.
- 758 56. Sherwood, J.J., Waller, G.S., Warshaw, D.M., and Lowey, S. (2004). A point mutation in the  
759 regulatory light chain reduces the step size of skeletal muscle myosin. *Proc National Acad Sci*  
760 **101**, 10973–10978.
- 761 57. Patterson, S.E., Mook, L.B., and Devoto, S.H. (2007). Growth in the larval zebrafish pectoral  
762 fin and trunk musculature. *Dev Dynam* **237**, 307–315.
- 763 58. Papatheodorou, I., Fonseca, N.A., Keays, M., Tang, Y.A., Barrera, E., Bazant, W., Burke,  
764 M., Füllgrabe, A., Fuentes, A.M.-P., George, N., et al. (2017). Expression Atlas: gene and  
765 protein expression across multiple studies and organisms. *Nucleic Acids Res* **46**, D246–D251.
- 766
- 767

768 **Figure Legends**

769

770 **Figure 1: Phenotypic Characteristics of Individuals with Recessive or Dominant Distal**

771 **Arthrogyriposis type 1 due to variants in *MYLPF*.**

772 **(A-C)** Characteristics shown in Family B II-1 with recessive DA1 A) camptodactyly of the fingers  
773 and radial deviation of the wrists. B,C) Gross pathology of the right foot illustrating absence of  
774 skeletal muscles. **(D-F)** Characteristics in Family H IV-1 with dominant DA1 D) [authors  
775 removed this image to comply with preprint server rules] pursed lips, camptodactyly of the  
776 fingers, adducted thumbs E) clinodactyly of the fifth digit F) bilateral clubfoot. Table 1 contains a  
777 detailed description of the phenotype of each affected individual and Figure S1 provides a  
778 pedigree of each family with DA1 due to variants in *MYLPF*.

779

780 **Figure 2: Genomic Model of *MYLPF***

781 *MYLPF* is composed of 7 exons, each of which consists of protein-coding (blue) and non-coding  
782 (orange) sequence. The approximate location of each pathogenic variant is indicated by an  
783 arrow. The p.(C157F) and p.(C157R) variants are each found in three families (x3) and lead to a  
784 recessive phenotype (purple circle). The p.(A33V) and p.(G163S) variants lead to a dominant  
785 phenotype (red circle).

786

787 **Figure 3: Zebrafish *mylpfa* mutants have weakened myotomes and paralyzed fin muscle.**

788 **(A-D)** RNA *in situ* hybridization showing (A, B) *mylpfa* and (C, D) *mylpfb* expression at 20 hpf  
789 (A, C) and 52 hpf (B, D). Both genes are expressed exclusively in fast muscle, including somitic  
790 muscles, fin muscle (green arrowhead), and posterior hypaxial muscle (red arrowhead). **(E)**  
791 Transcript abundance of *mylpfa* (blue) and *mylpfb* (orange) through early larval development,  
792 using data provided in the EMBL-EBI expression atlas.<sup>58</sup> **(F)** Alignment of wild-type (WT) and  
793 mutant genomic sequence across the *mylpfa*<sup>oz30</sup> and *mylpfa*<sup>oz43</sup> lesions. *mylpfa*<sup>oz30</sup> is a 20 bp

794 deletion within Exon 3 predicted to frameshift the 169 amino acid protein after amino acid 76,  
795 and *mylpfa*<sup>oz43</sup> is a 1 bp deletion within Exon 2 predicted to frameshift the protein after amino  
796 acid 52. **(G)** Diagram of wild-type and predicted mutant Mylpfa proteins. Both mutant alleles  
797 should truncate the protein within the first EF-hand domain (black boxes) and introduce short  
798 stretches of aberrant amino acids after the frameshift (brown). **(H)** Alignment of wild-type and  
799 predicted mutant proteins in the region of frameshift, showing normal sequence (black) and  
800 aberrant residues (brown). **(I)** Superimposed time-lapse images (from Movie S1) showing fin  
801 motion in a wild-type embryo (yellow crescent arrows) and motionless fins in a *mylpfa*<sup>oz30</sup> mutant  
802 (yellow dots) at 4 dpf. Similar results were obtained using a second mutant allele, *mylpfa*<sup>oz43</sup> (not  
803 shown). **(J)** Quantification of fin beats per minute averaged over left and right sides, in  
804 *mylpfa*<sup>oz30</sup> mutant (n=12) or phenotypically wild-type sibling (n=12) fish at 4 dpf. We have never  
805 observed a fin beat in over 100 *mylpfa*<sup>oz30</sup> and *mylpfa*<sup>oz43</sup> mutant fish examined. **(K)** Trunk  
806 muscle contractile force in *mylpfa*<sup>oz30</sup> and wild-type or heterozygous siblings at 3 dpf. No  
807 significant differences are found between wild-type and heterozygous fish. However,  
808 homozygous *mylpfa* mutant fish are significantly weaker than non-mutant siblings at all  
809 stimulation frequencies. **(L)** Representative image of fluorescently-labeled actin filaments  
810 tracked in the *in vitro* motility assay, with colored lines showing traces of individual filaments  
811 over 50 frames of imaging (2.5 seconds). Within this time period, actin filaments on wild-type  
812 myosin extracts typically move further than do filaments on *mylpfa* mutant myosin extracts. **(M)**  
813 Actin filament speeds measured using the *in vitro* motility assay generated by extracted myosin.  
814 Myosin from *mylpfa* homozygous mutant fish propel actin filaments significantly slower than  
815 myosin from wild-type siblings. Numbers shown in each bar indicate the experimental N; each  
816 experiment uses myosin extracted from two fish (see Methods). Asterisks indicate P thresholds  
817 for the WT/het pools vs mutant; \* indicates P<0.05, \*\* indicates p<0.001, \*\*\* indicates p<0.0001.  
818 Error bars represent standard deviation. Statistical comparisons in J and M use student's T test;

819 in K, thresholds are determined by ANOVA followed by Tukey-Kramer comparisons. Scale bar  
820 in I is 250  $\mu\text{m}$ .

821

822 **Figure 4: Embryonic muscle degenerates in *mylpfa* mutant zebrafish. (A, B)** Confocal

823 images showing muscle morphology at 26 hpf in wild-type (A) or *mylpfa*<sup>-/-</sup> (B) embryos.

824 Myonuclei are labeled using Rbfox1l immunolabeling (green), fast-twitch fibers are labeled using

825 F310 immunolabeling (red), and slow-twitch fibers are labeled using *Tg(smyhc1:EGFP)i104*

826 (blue). **(C, D)** Confocal z-sections showing muscle morphology of live 6 dpf larvae expressing a

827 fast muscle cell membrane transgene *Tg(mylpfa:lyn-Cyan)fb122* (green) and a myonuclear

828 transgene *myog:H2B-mRFP* (red). These fish also express a slow muscle marker

829 *Tg(smyhc1:EGFP)i104* (blue), which is largely lateral to the plane of focus; pink arrowheads

830 point to slow muscle cells within the shown plane. Compared to wild-type controls (C), *mylpfa*<sup>-/-</sup>

831 myofibers have irregular membrane structure (D). **(E, F)** Confocal projections of the same

832 sections from panels C and D showing slow muscle fibers (white). **(G-J)** Confocal projections of

833 pectoral fin and PHM muscles, imaged on 3.25 dpf and again on 4.25 dpf, in fish expressing

834 transgenes *Tg(mylpfa:lyn-Cyan)fb122* in fast muscle (green), *myog:H2B-mRFP* in all myonuclei

835 (red), and *Tg(smyhc1:EGFP)i104* in slow muscle (blue). Fin muscle and PHM express

836 *Tg(mylpfa:lyn-Cyan)fb122* but not *Tg(smyhc1:EGFP)i104*, as expected for muscles

837 predominantly comprised of fast-twitch fibers.<sup>23,57</sup> In striking contrast to wild-type (G, H), *mylpfa*

838 mutant muscle fibers degenerate between 3.25 and 4.25 dpf (I, J). **(K-M)** Images from a time-

839 lapse of *mylpfa* mutant PHM degeneration (Movie S3). Muscle fibers which initially appear wavy

840 (aqua outline), often become narrow (red arrowheads) before breaking apart (asterisk). A

841 myofiber that appears during imaging is outlined in magenta. Insets in C, D, G-J show

842 *Tg(mylpfa:lyn-Cyan)fb122* in greyscale. Scale bars in A (for A, B), E (for C-F), G (for G-J), and K

843 (for K-M) are 50  $\mu\text{m}$ .

844



845 **Figure 5: Mylpf protein sequence and structure comparisons identify key conserved**  
846 **residues. (A)** Model of rabbit Mylpf protein in complex with the neck and head region of myosin  
847 heavy chain in rigor. The heavy chain (cyan) and essential light chain (orange) are rendered  
848 using a space-filling model and the light chain is shown using a ball and stick model (yellow)  
849 except for three residues that align with MYLPF Ala33, Cys157, and Gly163, which are  
850 rendered in space filling models; we refer to these by their human numbering. Ala33 (green) is  
851 adjacent to a Lys residue in the heavy chain (white). Gly163 (magenta) directly contacts a Phe  
852 residue in the heavy chain (dark blue). In contrast, Cys157 (Red) is found internal to Mylpf  
853 protein. **(B)** Overview of myosin interaction with thin filaments, color-coded as in panel A. Mylpf  
854 protein binds to the heavy chain region that bends towards the thin filament (arrows). **(C)**  
855 Alignment of select vertebrate Mylpf proteins and invertebrate Myl2 proteins highlighting  
856 conservation of Ala33, Cys157, and Gly163. **(D-G)** Magnified views of myosin heavy and light  
857 chain genes showing how Ala33 and Gly163 positions vary between scallop<sup>40</sup> **(D)**, squid<sup>41</sup> **(E)**,  
858 chicken<sup>42</sup> **(F)**, and rabbit<sup>43</sup> **(G)**. Cys157 is located internally to the two vertebrate Mylpf  
859 structures (F, G). Color coding in panels D-G is the same as in panel A. **(H)** Alignment of human  
860 regulatory and essential light chain proteins highlighting conservation of Ala33, Gly163, and  
861 Cys157. The tissue that express each ortholog is indicated as follows: embryonic skeletal  
862 muscle (Emb), fast-twitch skeletal muscle (Fast), slow-twitch skeletal muscle (Slow), cardiac  
863 muscle (Card), and non-sarcomeric tissue (NS). The first residue in the shown aligned portions  
864 are numbered for each protein, and proteins are arranged by their similarity to MYLPF (C and  
865 H).

866

867

868 **Tables**

869 **Table 1. Mutations and Clinical Findings of Individuals with Distal Arthrogryposis type 1**  
870 **due to variants in *MYLPF***

871 This table provides a summary of clinical features of affected individuals from families in which  
872 mutations in *MYLPF* were identified. Clinical characteristics listed in the table are primarily  
873 features that delineate DA1. Plus (+) indicates presence of a finding, minus (-) indicates  
874 absence of a finding. \* = described per report. ND = no data were available. NA = not  
875 applicable. CADD = Combined Annotation Dependent Depletion v1.6. cDNA positions named  
876 using HGVS notation and RefSeq transcript NM\_002470.3. Predicted amino acid changes are  
877 shown.

**Table 1.**

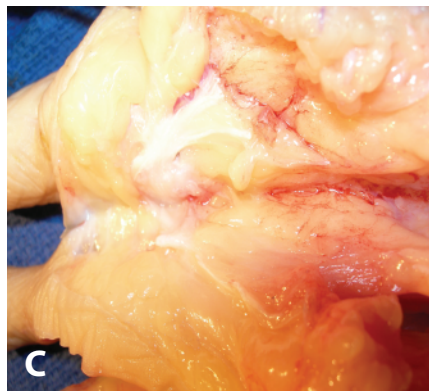
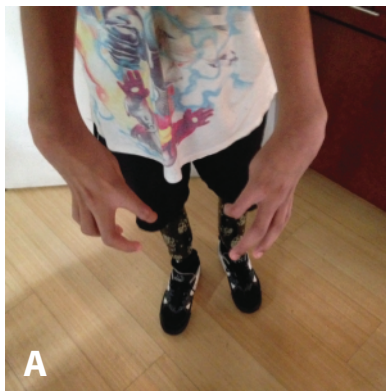
Family	A	A	B	C	D	E	F	F
Ancestry	Polish	Polish	Indian	Pakistani	Pakistani	Pakistani	Indian	Indian
Individual	VI-1	VI-2	II-1	II-1	IV-2	II-1	IV-8	IV-10
Sex	male	female	male	female	female	male	unknown	female
Age at last assessment	13 years	24 years	6.5 years	29 years	35 weeks	at birth (37+2 gestational weeks)	12 weeks gestation (antenatal ultrasound)	19 weeks gestation (perinatal autopsy)
<b>Variant</b>								
cDNA change	c.470G>T	c.470G>T	c.470G>T	c.469T>C	c.469T>C	c.469T>C	c.470G>T	c.470G>T
Genomic coordinates	chr16:g.30389181G>T	chr16:g.30389181G>T	chr16:g.30389181G>T	chr16:g.30389180T>C	chr16:g.30389180T>C	chr16:g.30389180T>C	chr16:g.30389181G>T	chr16:g.30389181G>T
CADD score	27.5	27.5	27.5	25.2	25.2	25.2	27.5	27.5
Amino acid change	p.Cys157Phe	p.Cys157Phe	p.Cys157Phe	p.Cys157Arg	p.Cys157Arg	p.Cys157Arg	p.Cys157Phe	p.Cys157Phe
Genotype	homozygous	homozygous	homozygous	homozygous	homozygous	homozygous	homozygous	homozygous
Inheritance	recessive	recessive	recessive	recessive	recessive	recessive	recessive	recessive
<b>Growth</b>								
Weight %ile	<1	8	8.8	<1	ND	3-10 (1820 g)	ND	50 (249 g)
Height %ile	1.1	ND	<1	<1	ND	ND	ND	48 (22 cm)
<b>Head and Neck</b>								
Small mouth	+	+	+	-	ND	-	-	retrognathia
Lip/palate	cleft lip & palate	cleft lip & palate	-	-	ND	-	ND	thin vermilion, bifid uvula
Neck	limited rotation	limited rotation	limited rotation	limited rotation	ND	short	increased nuchal translucency	short
<b>Skeletal</b>								
Scoliosis	+	+	+	+	ND	+	-	-
Short stature	+	+	+	+	+	ND	ND	-
Hip contractures	+	+	ND	+	ND	+	ND	+
Elbow contractures	+	+	-	+	ND	+	ND	-
Knee contractures	+	+	-	+	-	+	ND	+
Camptodactyly (fingers)	+	+	+	+	-	+	ND	+
Vertical talus	+	+	-	-	-	-	ND	-
Equinovarus	-	-	+	+	+	+	+	+
Camptodactyly (toes)	-	-	+	-	-	-	ND	-
Contractures of wrists	-	-	+	+	-	+	ND	ND
<b>Other</b>								
Undescended testicles	+	NA	+	NA	NA	-	ND	-

<b>Table 1. Continued</b>								
Family	F	F	G	G	H	H	H	H
Ancestry	Indian	Indian	Ashkenazi Jewish	Ashkenazi Jewish	French	French	French	French
Individual	III-2	III-3	II-1	III-1	IV-3	III-6	II-7	III-2
Sex	Female	Female	male	male	F	F	F	F
Age at last assessment	38 years	36 years	>18 years	1 year	6 years	39 years	69 years	26 years
<b>Variant</b>								
cDNA change	c.470G>T	c.470G>T	c.487G>A	c.487G>A	c.98C>T	c.98C>T	c.98C>T	c.98C>T
Genomic coordinates	chr16:g.30389181G>T	chr16:g.30389181G>T	chr16:g.30389198G>A	chr16:g.30389198G>A	chr16:g.30387467C>T	chr16:g.30387467C>T	chr16:g.30387467C>T	chr16:g.30387467C>T
CADD score	27.5	27.5	32.0	32.0	31.0	31.0	31.0	31.0
Amino acid change	p.Cys157Phe	p.Cys157Phe	p.Gly163Ser	p.Gly163Ser	p.Ala33Val	p.Ala33Val	p.Ala33Val	p.Ala33Val
Genotype	homozygous	homozygous	heterozygous	heterozygous	heterozygous	heterozygous	heterozygous	heterozygous
Inheritance	recessive	recessive	de novo	dominant	dominant	dominant	dominant	dominant
<b>Growth</b>								
Weight %ile	ND	ND	ND	<3rd	+1.5 SD	-0.5 SD	+0.5 SD	ND
Height %ile	ND	ND	ND	ND	+0.5 SD	-0.5 SD	0 SD	ND
<b>Head and Neck</b>								
			Head and Neck					
Small mouth	-	-	ND	+, limited opening	+	+	+	+
Lip/palate	-	thin vermilion	ND	high arched palate	-	-	-	pursed lips
Neck	-	-	ND	-	-	-	-	-
<b>Skeletal</b>								
Scoliosis	-	-	ND	-	-	-	-	+
Short stature	ND	ND	ND	ND	-	-	-	-
Hip contractures	-	-	ND	+	-	-	-	-
Elbow contractures	-	-	ND	-	-	-	-	-
Knee contractures	-	-	ND	+	-	-	-	-
Camptodactyly (fingers)	+	+	+	+	+	+	+	+
Vertical talus	ND	ND	ND	+	+	+	-	-
Equinovarus	-	+	ND	-	+	-	-	-
Camptodactyly (toes)	ND	ND	ND	+	-	-	-	-
Contractures of wrists	+	+	+	-	+	+	+	+
<b>Other</b>								
Undescended testicles	NA	NA	ND	+	NA	NA	NA	NA
					retrognathism, chin skin folds	shoulder contractures	shoulder contractures	adducted thumbs, flexed metacarpophalangeal joints, blepharophimosis

bioRxiv preprint doi: <https://doi.org/10.1101/2020.05.06.071555>; this version posted May 8, 2020. The copyright holder for this preprint (which was not certified by peer review) is the author/funder, who has granted bioRxiv a license to display the preprint in perpetuity. It is made available under aCC-BY-ND 4.0 International license.

**Table 1. Continued**

Family	H
Ancestry	French
Individual	IV-1
Sex	M
Age at last assessment	6 months
<b>Variants</b>	
cDNA change	c.98C>T
Genomic coordinates	chr16:g.30387467C>T
CADD score	31.0
Amino acid change	p.Ala33Val
Genotype	heterozygous
Inheritance	dominant
<b>Growth</b>	
Weight %ile	-1SD
Height %ile	0SD
<b>Facial features</b>	
Small mouth	+
Lip/palate	pursed lips, high arched palate
Neck	-
<b>Skeletal</b>	
Scoliosis	-
Short stature	-
Hip contractures	-
Elbow contractures	-
Knee contractures	-
Camptodactyly (fingers)	+
Vertical talus	-
Equinovarus	+
Camptodactyly (toes)	-
Contractures of wrists	+
<b>Other</b>	
Undescended testicles	ND
	adducted thumbs, flexed metacarpophalangeal joints, fifth finger clinodactyly

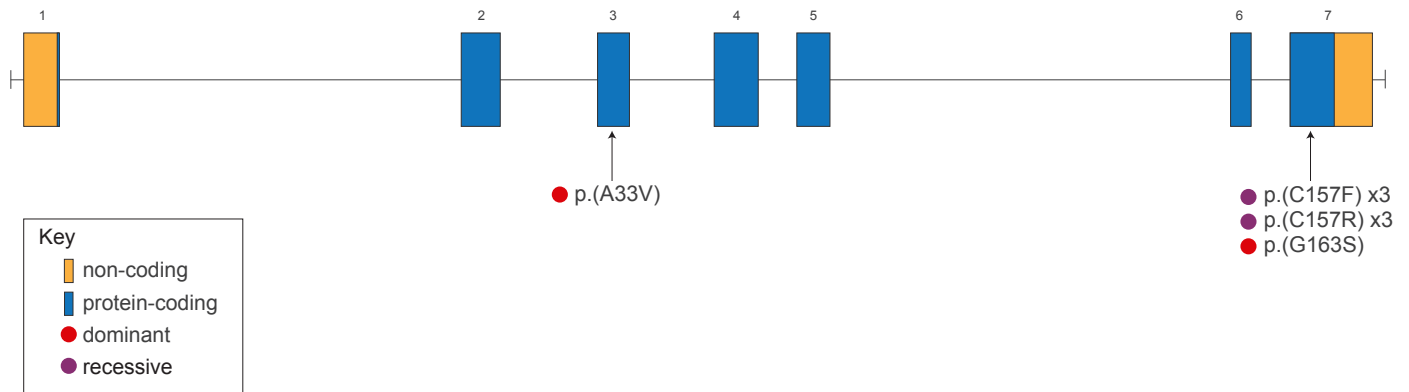


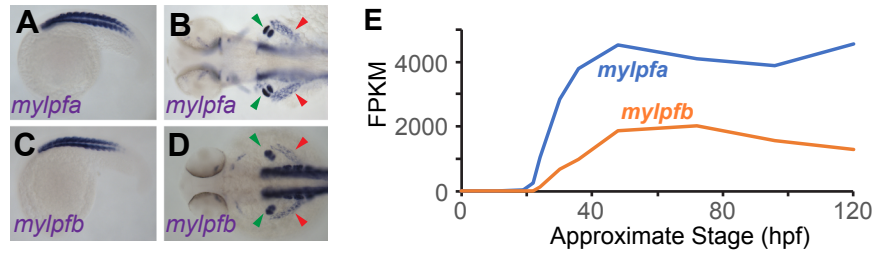
**D**

Authors omitted this image to comply with preprint server rules



## MYLPF





**F** WT *mylpfa* c.225 CAGCGGCCCAATCAACTTCACCGTTTT  
*mylpfa*<sup>oz30</sup> c.225 CAGC-----TTT

WT *mylpfa* c.150 CCTTAG-GGACGTG  
*mylpfa*<sup>oz43</sup> c.150 CCTTAGACGACGTG



**H** WT *mylpfa* p.73 KEASGPINFTVFLTMFG WT *mylpfa* p.49 DDLRDVLASMGQLN  
*mylpfa*<sup>oz30</sup> p.73 KEASFPHHVRRVEGC\* *mylpfa*<sup>oz43</sup> p.49 DDLRRRVGLNGPA\*

